

Decoupling Ionic and Electronic Pathways in Low-Dimensional Hybrid Conductors

Yubing Zhou,^{†,⊥} Chaoji Chen,^{†,⊥} Xin Zhang,^{†,⊥} Dapeng Liu,[†] Lisha Xu,[†] Jiaqi Dai,[†] Sz-Chian Liou,[‡] Yilin Wang,[†] Claire Li,[†] Hua Xie,[†] Qingyun Wu,[†] Bob Foster,[§] Teng Li,^{||} Robert M. Briber,[†] and Liangbing Hu^{*,†,⊥}

[†]Department of Materials Science and Engineering, University of Maryland, College Park, Maryland 20742, United States

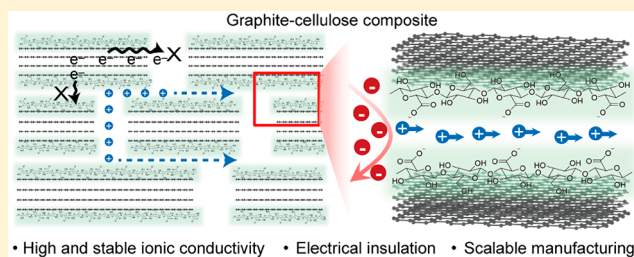
[‡]Advanced Imaging and Microscopy (AIM) Lab of Nano Center, University of Maryland, College Park, Maryland 20742, United States

[§]Trinity Industries, Inc., Dallas, Texas 75207, United States

^{||}Department of Mechanical Engineering, University of Maryland, College Park, Maryland 20742, United States

Supporting Information

ABSTRACT: The construction of two-dimensional (2D) layered compounds for nanofluidic ion transport has recently attracted increasing interest due to the facile fabrication, tunable channel size, and high flux of these materials. Here we design a nacre-mimetic graphite-based nanofluidic structure in which the nanometer-thick graphite flakes are wrapped by negatively charged nanofibrillated cellulose (NFC) fibers to form multiple 2D confined spacings as nanochannels for rapid cation transport. At the same time, the graphite–NFC structure exhibits an ultralow electrical conductivity ($\sigma_e \leq 10^{-9}$ S/cm), even when the graphite concentration is up to 50 wt %, well above the percolation threshold (~ 1 wt %). By tuning the hydration degree of graphite–NFC composites, the surface-charge-governed ion transport in the confined ~ 1 nm spacings exhibits nearly 12 times higher ionic conductivity (1×10^{-3} S/cm) than that of a fully swollen structure (~ 1.5 nm, 8.5×10^{-5} S/cm) at salt concentrations up to 0.1 M. The resulting charge selective conductor shows intriguing features of both high ionic conductivity and low electrical conductivity. Moreover, the inherent stability of the graphite and NFC components contributes to the strong functionality of the nanofluidic ion conductors in both acidic and basic environments. Our work demonstrates this 1D–2D material hybrid system as a suitable platform to study nanofluidic ion transport and provides a promising strategy to decouple ionic and electronic pathways, which is attractive for applications in new nanofluidic device designs.



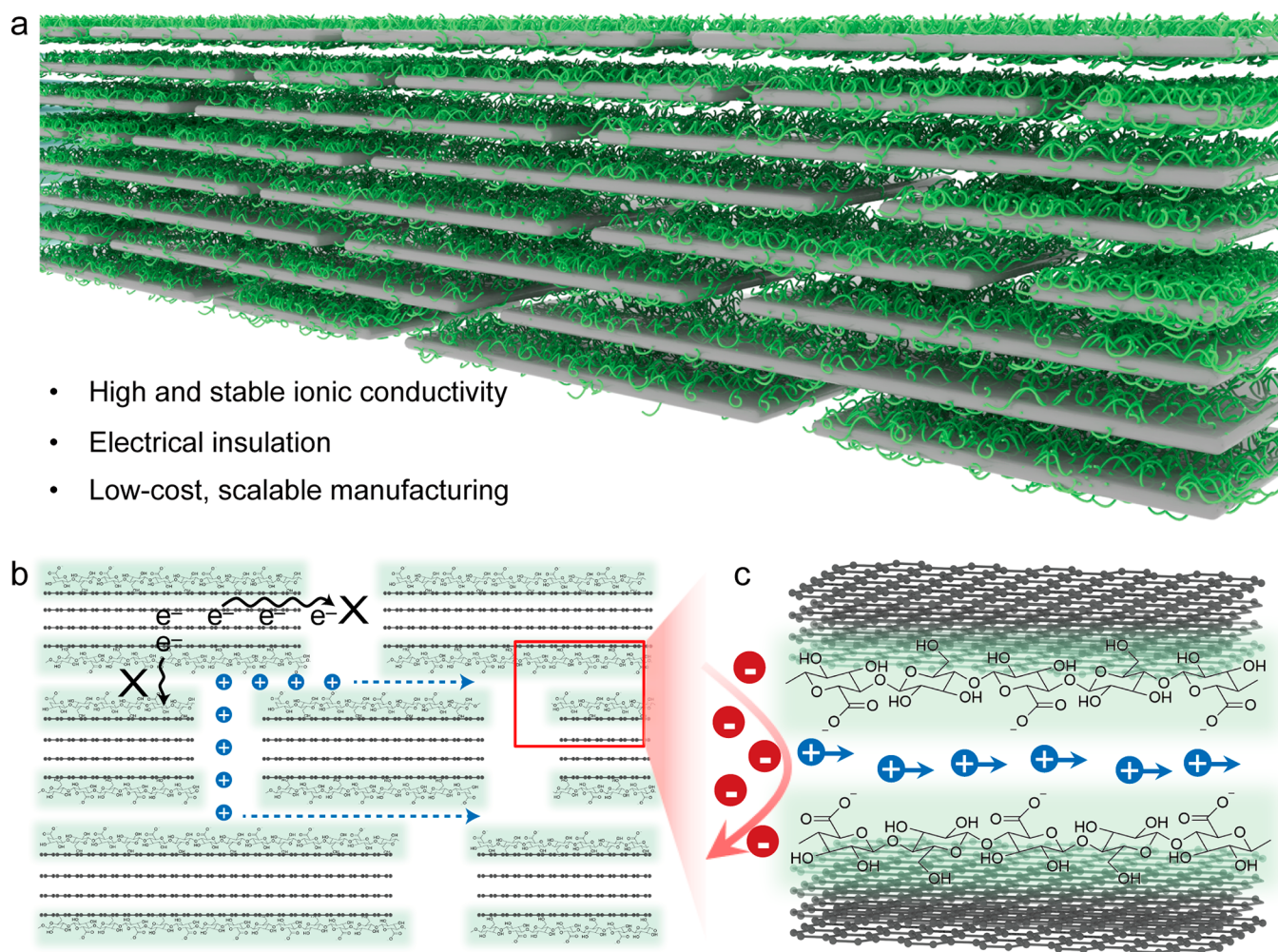
INTRODUCTION

Rapid ion transport is crucial for essential functions in living creatures and is also desired in innovative applications that span energy utilization,^{1–7} biosensing,^{8–11} and water treatment.^{12–14} The transport of fluids in geometries with characteristic nanoscale dimensions shows behaviors that significantly differ from their bulk counterparts.^{15–17} When the dimensions of the fluidic channels decrease to as low as the Debye length, the surface charge on the channel walls starts to dominate the ionic behaviors, with only ions of the opposite charge moving through due to electrostatic forces. Governed by this surface charge effect, the ionic conductivity at low salt concentrations is significantly higher in nanofluidic channels compared to that of bulk solution.^{18–21} Several methods have been demonstrated for the fabrication of such channels, including soft-template^{22–25} and photolithography-based^{26,27} techniques, but these artificial nanofluidic systems are far from real-world applications due to their complex fabrication processes, high cost, and low efficiencies.

To address these challenges, the construction of nanofluidic channels in two-dimensional (2D) material-based membranes through nonlithography approaches has been recently demonstrated.^{28–32} Two-dimensional layered materials, such as graphene oxide (GO) and boron nitride (BN), have been assembled into nanofluidic membranes via a facile filtration process.^{20,29} The layered structures of these 2D materials facilitate the fabrication of large-scale nanofluidic devices, which was proved in restacking exfoliated GO sheets by Raidongia and Huang in 2012.²⁰ Outstanding ion transport properties were confirmed through the densely stacked 2D nanosheets. However, most of these 2D nanosheets suffer from either scale-limited fabrication (solution process with a low solid content, chemical vapor deposition growth, etc.) or poor thermal, chemical, and mechanical stability (e.g., thermal reduction of GO at a relatively low temperature).^{33–36} Nanofluidic devices combining nanoscale channels with good

Received: August 20, 2019

Published: October 24, 2019



- High and stable ionic conductivity
- Electrical insulation
- Low-cost, scalable manufacturing

Figure 1. (a) Schematic of the proposed microstructure for the printed graphite–NFC composite. (b) Graphite flakes and NFC fibers are alternately stacked into a layered structure. (c) Debye layers of neighboring graphite flakes overlap to create 2D nanofluidic channels that enable selective ion transport of positive ions.

material stability and large-scale manufacturing have yet to be achieved. As a result, scalable and controllable manufacturing of robust nanofluidic ion conductors has remained challenging.

In this work, we present the scalable fabrication of graphite-based nanofluidic ion conductors via nanofibrillated cellulose (NFC)-assisted exfoliation, which exhibits high ionic conductivities and excellent chemical and thermal stability. The material design is inspired by the microstructure of the nacreous part in seashells, which has an alternatively layered arrangement of hard inorganic layers (i.e., graphite flakes) and soft polymers (i.e., NFC fibers) (Figure 1a). This nature-inspired lamellar structure demonstrates facile and scalable fabrication as well as highly tunable, massive nanochannels. The NFC chain has a flat ribbon-like conformation composed of ringed glucose molecules.³⁷ NFC fibers attach to the graphite flakes through the interaction between its hydrophobic sites and the hydrophobic surface of graphite flakes, as well as hydrogen bonding between the NFC hydroxyl groups and the defective edges of the graphite flakes. The interstitial space between adjacent graphite flakes separated by the NFC fibers can be treated as lamellar channels for charge transport. Due to the wrapping of individual graphite flake by NFC in the graphite–NFC composite, electronic transmission can be completely blocked (Figure 1b), and the electronic con-

ductivity of the graphite–NFC composite is less than 10^{-9} S/cm, even when the graphite concentration is high (~ 50 wt %) and well above the percolation threshold (typically ~ 1 wt %). At the same time, the plateau ionic conductivity at low salt concentrations (up to 0.1 M) is $\sim 1 \times 10^{-3}$ S/cm. As the existing negatively charged carboxyl group on the NFC chains after (2,2,6,6-tetramethylpiperidin-1-yl)oxidanyl (TEMPO) treatment, the nanofluidic channels can selectively exclude ions with the same charge and attract ions of the opposite charge (Figure 1c, zeta potential = -51.5 mV, pH = 7; Figure S1).^{38,39} This electrically insulating yet ionically conductive graphite–NFC composite provides an ideal platform for investigating the dependency of the ion transport behavior on the nanochannel spacing in a large-scale material system, which also holds great promise for a wide range of potential applications, such as energy storage and conversion, membrane separation, ionic circuits, and desalination.

RESULTS AND DISCUSSION

To fabricate the graphite–NFC composite, we prepared NFC fibers using a top-down approach from wood cell walls and used them to disperse graphite flakes via sonication. NFC features both hydrophilic functional groups and hydrophobic C–H moieties, which allow it to be used as a dispersant^{40,41} to

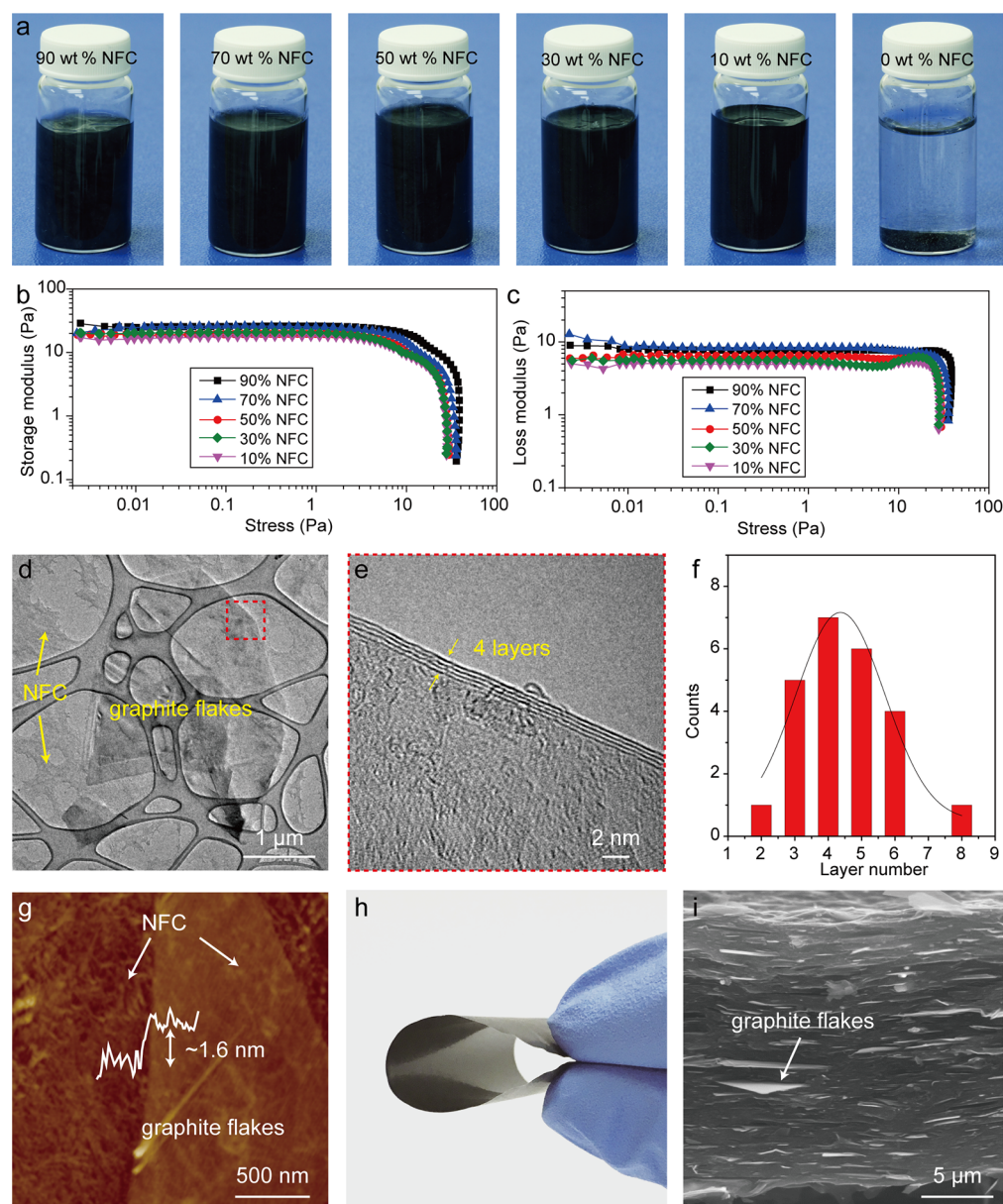


Figure 2. (a) Images of graphite nanoflakes dispersed in water without NFC and with different weight percentages of NFC (10–90 wt %). (b, c) Storage modulus (b) and loss modulus (c) as a function of the oscillation stress (Pa) for the graphite–NFC slurries made with various NFC weight percentages. (d) Low-magnification TEM image of individual graphite flakes wrapped by NFC. (e) Corresponding high-resolution TEM image of the folded edge of the graphite flake. (f) Layer number distribution histogram for graphite flakes obtained from 24 samples. (g) AFM image of a graphite flake wrapped by NFC. The NFC fibers adsorb on the surface of the graphite flake. (h) A flexible graphite–NFC film can be obtained after drying. (i) Cross-sectional SEM image to show the lamellar structure of the graphite–NFC film in (h).

direct exfoliation of graphite into a homogeneous aqueous solution of 2D nanoflakes.⁴² The NFC-assisted graphite dispersion clearly demonstrates better stability compared to that without NFC, which falls out of solution almost immediately (Figure 2a). Furthermore, the graphite can be dispersed well with only 10 wt % NFC, which is a much lower mass ratio than previously reported surfactant-assisted dispersions.⁴³ Figure 2b and c compare the storage modulus (G') and loss modulus (G'') of the graphite–NFC slurry as a function of shear stress at different NFC mass ratios from 10 to 90 wt % at a fixed amount of NFC. The G' and G'' values of the slurries increased slightly as the NFC mass ratio increased substantially, indicating that the concentration of NFC dominates the rheological behaviors of the slurries.

Figure 2d shows a typical low-magnification transmission electron microscopy (TEM) image of the ultrathin graphite nanoflakes supported by the lacey carbon film, showing how the exfoliated few-layer graphite flake is wrapped in NFC fibers. From the corresponding high-resolution TEM image of a folded edge of the graphite flake, a four-layer structure with periodical fringes is clearly visible (Figure 2e). The alternating bright and dark fringes indicate the graphite layer number, with most flakes exhibiting 3–6 layers of graphene (Figure 2f). An atomic force microscopy (AFM) image shows that the NFC fibers are closely associated with the surface of the graphite flake. The thickness of the graphite flakes obtained from the height profile (~ 1.6 nm) can be used to calculate the layer numbers (~ 4 layers) (Figure 2g). With the moisture loss and a

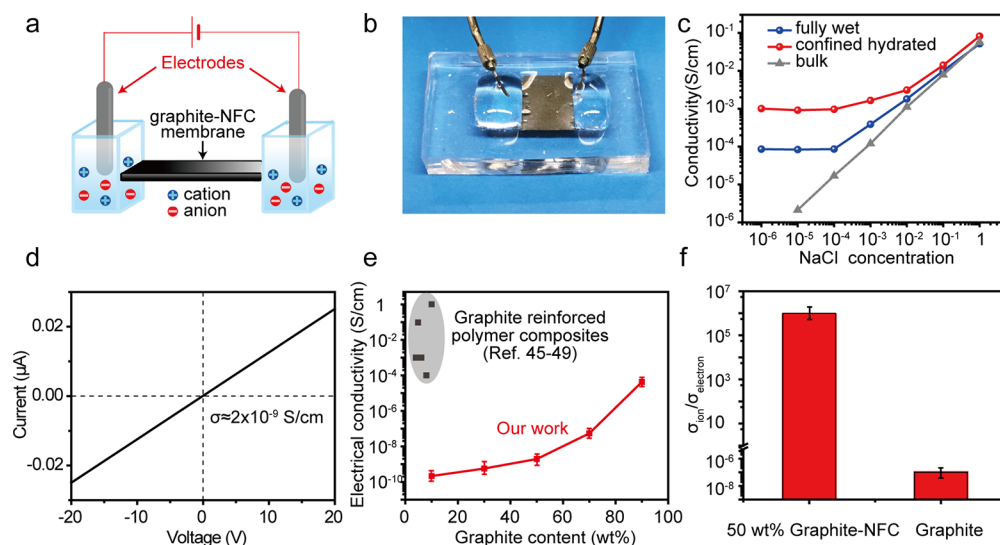


Figure 3. (a) Schematic illustration and (b) photograph showing the graphite–NFC membrane-based nanofluidic device. (c) Ionic conductivity as a function of electrolyte concentration at different NaCl concentrations. The blue and red lines are the ionic conductivities of the fully wet and confined hydrated graphite–NFC nanofluidic devices, respectively. (d) Representative I – V curve of the graphite–NFC membrane (1:1 mass ratio). (e) Electrical conductivity vs graphite content of the graphite–NFC membrane. The literature data (black dots) show that most graphite-reinforced polymer composites demonstrate electrical conductivities higher than 10^{-4} S/cm even at carbon loadings below 10 wt %.^{45–49} Our work exhibits preferable low electric conductivities for ion transport purposes. (f) Ratio of the ionic conductivity to electrical conductivity of our 50 wt % graphite–NFC composite and pure graphite.

hot press process, the graphite–NFC slurry (1:1 mass ratio) forms a densely stacked multilayered membrane that can be easily peeled off from the substrate (Figure 2h). We also characterized the micromorphology of the graphite–NFC membrane using scanning electron microscopy (SEM). Figure 2i reveals the layered, nacre-mimetic structure of the graphite flakes and NFC, confirming the successful hydrodynamic self-ordering of the NFC-coated flakes during water removal (Figure S2).

Typical nanofluidic devices were fabricated using the graphite–NFC membranes (1:1 mass ratio), as illustrated in Figure 3a. After sealing the rectangular membranes with epoxy resin, the two ends were exposed to the electrolyte in order to conduct two terminal measurements (Figure 3b). Graphite–NFC membranes in dry and fully wet states were embedded in epoxy to study the dependence between the height of the nanochannels and the ionic conductivities. After sufficiently soaking in water for several days, the membranes are fully hydrated but still confined by the epoxy. Then the devices were immersed in the electrolytes for 24 h to obtain a stable current at different electrolyte concentrations. The thickness of the membrane is preserved by the epoxy after soaking and ensures the dimensional stability of the samples during the ionic conductivity tests as ions are driven through the continuous nanofluidic channels when a voltage is applied. On the basis of the resulting I – V curves at various NaCl concentrations (Figures S3), we calculated the corresponding ionic conductivities (Figure 3c). The conductivity of the bulk NaCl solution is proportional to the concentration due to the free migration of ions in bulk solution (Figure 3c, gray dashed line). For the ionic conductivity of the graphite–NFC conductors (Figure 3c, blue and red circles), the data points almost coincide with those of the bulk at concentrations higher than 0.1 M. However, the ionic conductivity starts to deviate from the bulk values when the NaCl concentration is below 0.1 M. For the graphite–NFC membranes, ion transport in the

nanochannels is dominated by surface charge rather than bulk electrolyte concentration until the ion concentration is lower than 1×10^{-4} M, with a constant value of $\sim 1 \times 10^{-3}$ S/cm for the confined hydrated state membrane (red circles) and 9×10^{-5} S/cm for the fully wet one (blue circles). The space between the graphite flakes forms 2D nanofluidic channels for water and cation transport. When the Debye length is larger than the interlayer spacing, the cations become the dominant charge carriers.⁴⁴ As a result of this surface-charge-governed transport mechanism, the graphite–NFC membranes display higher ion conductivity than in bulk solution. Meanwhile, the increased nanochannel height in the wet-swollen graphite–NFC membranes leads to a lower ionic conductivity.

To gain insight into the electrical conductivity of the graphite–NFC membranes when dry, we extracted the representative I – V output curve. Figure 3d shows the I – V characteristic of the graphite–NFC membranes (1:1 mass ratio), which indicates an electrical conductivity of 2×10^{-9} S/cm. The NFC fibers wrapping around the 2D graphite flakes endow the graphite–NFC composite with electrically insulating properties. Furthermore, we found the graphite–NFC membranes maintain this electrical insulation even at graphite concentrations as high as 50 wt %, which guarantees that solely ions will be transported (Figure 3e). Carbon materials (e.g., carbon nanotubes and graphene) in polymers generally demonstrate several orders of magnitude higher electric conductivities than 10^{-4} S/cm even at loadings below 10 wt %.^{45–49} As a result, they have limited use in electrolytes, as they can cause electrical short circuits. Meanwhile, in our graphite–NFC composites, the graphite flakes are embedded within insulating NFC layers, enabling a high ionic conductivity along with an extremely low electrical conductivity even at a record high graphite content of 50 wt % (Figure 3f).

The NFC fibers play a key role in the nanofluidic ion conductors in terms of guaranteeing the surface-charge-

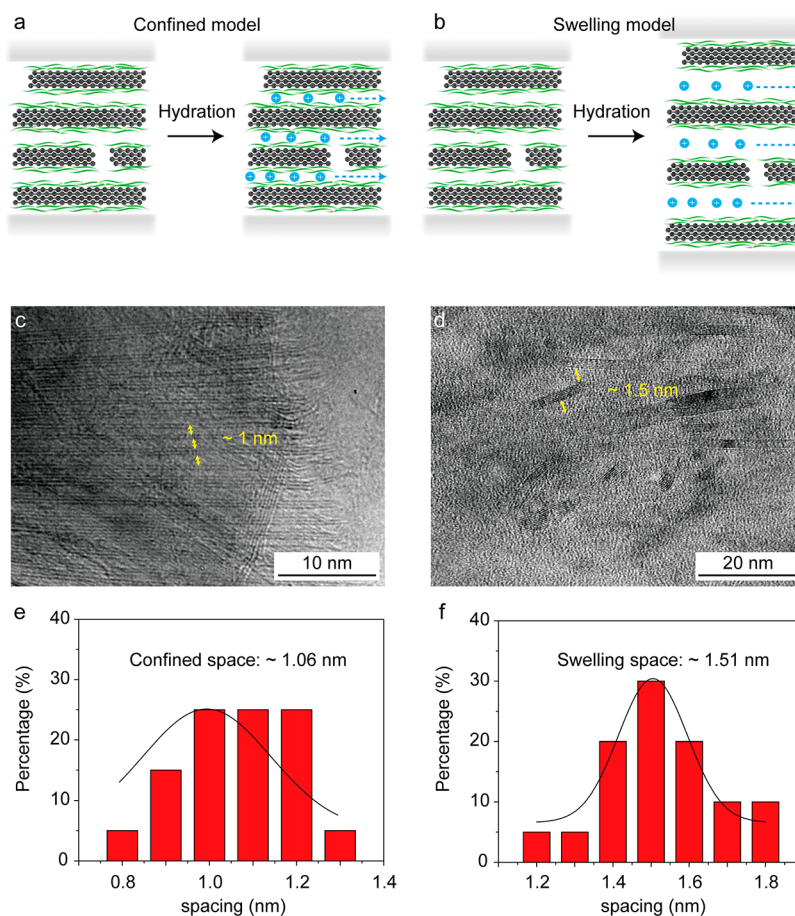


Figure 4. To better understand the channel formation in the graphite–NFC composite, the arrangement of the graphite flakes was explored using TEM. (a, b) Schematics of the nanofluidic channels of the graphite–NFC membrane in (a) the confined hydrated state and (b) the swelling state. (c, d) TEM images of the cross-section of a graphite–NFC film in the (c) confined hydrated state and (d) swelling state. (e, f) Histograms of the interlayer spacing distribution for graphite flakes in the (e) confined hydrated state and (f) swelling state.

governed ion transport and eliminating the risk of electrical shorting. As NFC features abundant oxygenated functional groups, the fibers have a strong tendency to absorb water and swell, which significantly affects the spacing between the adjacent graphite flakes and plays a key role in determining the ionic conductivity of the graphite-based conductors. Due to the hydrophilic nature of cellulose, the graphite–NFC membrane will swell in water when there is no external restriction (Figure 4a and b). The water-swollen graphite–NFC membrane is determined to have a total thickness increase of approximately 3 times compared to the dry state. To better understand the channel formation in the graphite–NFC composite (1:1 mass ratio), we investigated the spacing between the orderly stacked graphite flakes in the swelling and confined hydrated states using TEM. Thin sections of graphite–NFC composite embedded in epoxy were cut with an ultramicrotome, and the sectioned samples were mounted onto a copper grid for TEM observation. Figure 4c depicts a TEM image of the cross-section of the confined, hydrated graphite–NFC film. It is obvious that the bulk graphite was exfoliated into few-layer graphite flakes with good alignment, and the interlayer spacing can be observed clearly (Figure S4). We investigated more than 10 samples to obtain the statistical distribution of the interlayer spacing between the exfoliated graphite flakes (Figure S5). Graphite–NFC membranes swell when interflake spacing increases, allowing water to rapidly

penetrate the membrane through the voids. Subsequently, swelling occurs as water wets the NFC surfaces and continues to fill and create more space between the graphite flakes. This added space increases the thickness of the material, as confirmed by the changed microstructure in Figure 4d. The spacing between the orderly stacked graphite flakes wrapped by NFC is ~1.06 nm in the confined hydrated state (Figure 4e) and extends to ~1.51 nm in the water-swollen state (Figure 4f). The ionic conductivity (σ_{ion}) is calculated based on the equation $\sigma_{\text{ion}} = G(l/hw)$, in which G is the measured conductance (i.e., the slope of the I – V curve) and l , h , and w are the length, height, and width of the channels, respectively. The expansion of the spacing between the stacked graphite flakes in the swollen state leads to the increase in h , which is one of the reasons why the plateau in the ionic conductivity at low concentration decreased. The exfoliation of graphite into nanoflakes by the NFC also contributes to the high ionic conductivity, due to the construction of more nanofluidic channels (Figure S6a–d). The ions transporting through the exfoliated graphite nanofluidic channels exhibit 10 times higher conductivity than those of membranes made with graphite and NFC without sonication (Figure S6e,f).

Regarding the ion selectivity between ions of the same charge or between monovalents and divalents, there have been previous efforts to tune the interlayer spacing between 2D material sheets for precise ionic sieving in aqueous

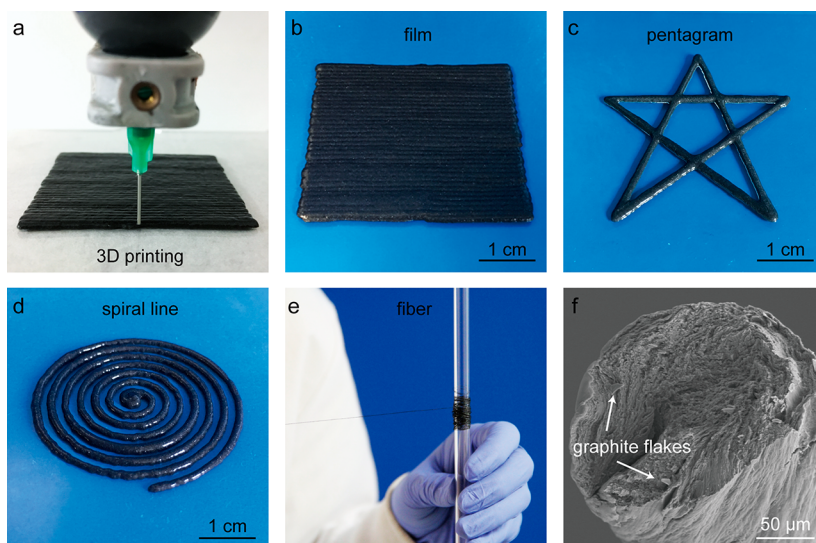


Figure 5. (a) The 3D printing process of the graphite–NFC slurry, which can be used to print (b) square, (c) pentagram, and (d) spiral shapes. (e) A long fiber printed from the graphite–NFC slurry that features a lamellar structure, as shown in the cross-sectional SEM image in (f).

solution.^{14,50} Nanochannels with sizes comparable to, or smaller than, the diameter of hydrated ions are predicted to show enhanced ion selectivity. The interlayer spacing of a 2D material laminar membrane, analogous to the pore size in polymer membranes, plays a significant role in its ion separation performance. For example, to achieve a small enough interlayer spacing, Abraham et al.¹⁴ designed GO laminates with a tunable interlayer spacing (from ~ 9.8 Å to 6.4 Å) by encapsulating the GO sheets in epoxy films. The capillary size is smaller than the hydrated diameters of ions (the hydrated diameters considered for K^+ , Na^+ , Ca^{2+} , and Mg^{2+} are 6.6, 7.1, 8.2, and 8.5 Å, respectively), and their permeation is exponentially suppressed with decreasing interlayer spacing, thus resulting in 97% NaCl rejection.¹⁴ In another study, Chen et al.⁵⁰ designed a facile and precise control of interlayer spacing in GO laminates to achieve accurate ion sieving. By regulation of interlayer spacing with ångström precision through using K^+ , Na^+ , Ca^{2+} , Li^+ , or Mg^{2+} ions, membrane spacings controlled by one type of cation can efficaciously and precisely exclude other cations that have larger hydrated volumes.⁵⁰

In our material system, the spacing between graphite flakes wrapped by NFC is ~ 1.06 nm in the confined hydrated state, which is larger than the hydrated diameters of K^+ , Na^+ , Ca^{2+} , and Mg^{2+} ions (6.6, 7.1, 8.2, and 8.5 Å, respectively). Due to the difficulties in fabricating graphite–NFC membranes with well-defined sub-nanometer channels, the realization of membranes with ion sieving would be a significant step forward. Although this is a great challenge, more efforts will be dedicated to decreasing the interlayer spacing of our composite material to realize the ion-sieving effect in our future study.

Our approach enables the formation of an aqueous graphite–NFC slurry with a solid content as high as 20 wt % due to the presence of adsorbed NFC fibers on the surface of the graphite flakes, which prevents them from restacking. The resulting solution features high viscosity and shear-thinning behavior, which enables it to be 3D printed (Figure S7). Extrusion-based 3D printing, a typical technique that builds structures by driving materials out of a nozzle and onto a stage, can be leveraged in preparing sophisticated patterns with superior control over material properties across multiple

dimensions, while remaining relatively cheap and easy to use.⁵¹ The shear-thinning graphite–NFC slurry, which exhibits a viscoelastic response to applied pressure, can be extruded from a nozzle to directly fabricate a 3D object (Figures 5a and S8).⁵² As NFC-based materials possess favorable rheological properties and excellent dimensional stability, various sophisticated geometries with a uniform printing diameter can be printed (Figure 5b–d). Additionally, graphite–NFC composite fibers of up to two meters in length with a diameter of ~ 200 μm can also be created (Figure 5e). The well-ordered, densely stacked graphite flakes in the cross-section of the fiber indicate the excellent alignment of the composite (Figures 5f and S9).

Since the graphite flakes retain their intrinsic carbon hexagonal bonding network after the mild NFC exfoliation process, excellent thermal and chemical stability is expected in the graphite–NFC nanofluidic device. To explore the chemical stability of this material, we conducted ionic conductivity tests in highly acidic and basic environments, with the concentration of HCl or KOH of up to 1 M (Figure S10a–d). Similar surface-charge governed ionic conductivity behaviors were observed at low concentrations (<0.1 M) in both HCl and KOH solutions and can be repeated. The graphite–NFC composites are thermally stable up to ~ 225 °C in air atmosphere, which was examined using thermogravimetric analysis (TGA) (Figure S11). To study the effect of temperature on the ionic conductivity, a graphite–NFC membrane, which had been fully hydrated in 0.1 mM HCl, was embedded by the epoxy with a thermometer near the membrane, and the device was heated in an oil bath. The ionic conductivity of the graphite–NFC membrane follows an Arrhenius behavior, as shown in Figure S10e and f. On the basis of these curves, we estimated the activation energy to be 0.08 eV, suggesting that proton transport in the graphite–NFC membrane follows a Grotthuss mechanism.^{53,54} As the protons can interact with the surrounding molecules or channel surface, the Grotthuss-like transport allows the coordinated hopping of protons between water molecules in the nanofluidic channels. The outstanding chemical and thermal stability of the graphite flakes enable the graphite–NFC nanofluidic device to function well in acidic, basic, and high-temperature environments.

CONCLUSION

In this work, we successfully designed and fabricated a graphite–NFC composite that features a high rate of ionic transport, excellent material stability, and scalable manufacturing for the production of nanofluidic devices. The exfoliation of graphite into nanoflakes by NFC fibers leads to the formation of a graphite–NFC composite with atomic level 1D–2D material hybridization and abundant nanoscale confined spaces that serve as nanofluidic channels for ionic transport. Because of the rich negatively charged surface functional groups and exceptional continuity of the 2D channels, the graphite–NFC membranes featured a much higher ionic conductivity at low salt concentrations (<0.1 M) than that in bulk solution, which is a signature of surface-charge-governed ionic transport. The confined graphite–NFC membrane with smaller nanofluidic spacing also shows more than 1 order of magnitude higher ionic conductivity (1×10^{-3} S/cm) than that of the fully swollen one (8.5×10^{-5} S/cm). In addition, the graphite–NFC nanofluidic ion conductors possess outstanding thermal and chemical stability under high temperature and extreme pH conditions. The highly ionic conductive, electrically insulating graphite–NFC structure with outstanding manufacturing capability can have applications in ionic devices, such as batteries and fuel cells.

ASSOCIATED CONTENT

Supporting Information

The Supporting Information is available free of charge on the ACS Publications website at DOI: 10.1021/jacs.9b09009.

Experimental details, more characterization results, additional figures of SEM and TEM images (PDF)

AUTHOR INFORMATION

Corresponding Author

*binghu@umd.edu

ORCID

Chaoji Chen: 0000-0001-9553-554X

Liangbing Hu: 0000-0002-9456-9315

Author Contributions

[†]Y. Zhou, C. Chen, and X. Zhang contributed equally to this work.

Notes

The authors declare no competing financial interest.

ACKNOWLEDGMENTS

We acknowledge the support of the Maryland Nanocenter, its Surface Analysis Center, and AIMLab.

REFERENCES

- (1) Yuan, Z.; Zhu, X.; Li, M.; Lu, W.; Li, X.; Zhang, H. A highly ion selective zeolite flake layer on porous membranes for flow battery applications. *Angew. Chem.* **2016**, *128* (9), 3110–3114.
- (2) Guo, W.; Cao, L.; Xia, J.; Nie, F. Q.; Ma, W.; Xue, J.; Song, Y.; Zhu, D.; Wang, Y.; Jiang, L. Energy harvesting with single ion selective nanopores: a concentration gradient driven nanofluidic power source. *Adv. Funct. Mater.* **2010**, *20* (8), 1339–1344.
- (3) Daiguji, H.; Yang, P.; Szeri, A. J.; Majumdar, A. Electrochemomechanical energy conversion in nanofluidic channels. *Nano Lett.* **2004**, *4* (12), 2315–2321.
- (4) Zhang, Z.; Sui, X.; Li, P.; Xie, G.; Kong, X.-Y.; Xiao, K.; Gao, L.; Wen, L.; Jiang, L. Ultrathin and ion-selective Janus membranes for

high-performance osmotic energy conversion. *J. Am. Chem. Soc.* **2017**, *139* (26), 8905–8914.

(5) Wang, M.; Meng, H.; Wang, D.; Yin, Y.; Stroeve, P.; Zhang, Y.; Sheng, Z.; Chen, B.; Zhan, K.; Hou, X. Dynamic Curvature Nanochannel Based Membrane with Anomalous Ionic Transport Behaviors and Reversible Rectification Switch. *Adv. Mater.* **2019**, *31* (11), 1805130.

(6) Xin, W.; Zhang, Z.; Huang, X.; Hu, Y.; Zhou, T.; Zhu, C.; Kong, X.-Y.; Jiang, L.; Wen, L. High-performance silk-based hybrid membranes employed for osmotic energy conversion. *Nat. Commun.* **2019**, *10* (1), 3876.

(7) Zhu, Y.; Zhan, K.; Hou, X. Interface design of nanochannels for energy utilization. *ACS Nano* **2018**, *12* (2), 908–911.

(8) Hou, X.; Jiang, L. Learning from nature: building bio-inspired smart nanochannels. *ACS Nano* **2009**, *3* (11), 3339–3342.

(9) Vlasiouk, I.; Kozel, T. R.; Siwy, Z. S. Biosensing with nanofluidic diodes. *J. Am. Chem. Soc.* **2009**, *131* (23), 8211–8220.

(10) Lemay, S. G. Nanopore-based biosensors: the interface between ionics and electronics. *ACS Nano* **2009**, *3* (4), 775–779.

(11) Chen, S.; Tang, Y.; Zhan, K.; Sun, D.; Hou, X. Chemiresistive nanosensors with convex/concave structures. *Nano Today* **2018**, *20*, 84–100.

(12) Kim, S. J.; Ko, S. H.; Kang, K. H.; Han, J. Direct seawater desalination by ion concentration polarization. *Nat. Nanotechnol.* **2010**, *5* (4), 297.

(13) Han, Y.; Xu, Z.; Gao, C. Ultrathin graphene nanofiltration membrane for water purification. *Adv. Funct. Mater.* **2013**, *23* (29), 3693–3700.

(14) Abraham, J.; Vasu, K. S.; Williams, C. D.; Gopinadhan, K.; Su, Y.; Cherian, C. T.; Dix, J.; Prestat, E.; Haigh, S. J.; Grigorieva, I. V. Tunable sieving of ions using graphene oxide membranes. *Nat. Nanotechnol.* **2017**, *12* (6), 546.

(15) Van Den Berg, A.; Craighead, H. G.; Yang, P. From microfluidic applications to nanofluidic phenomena. *Chem. Soc. Rev.* **2010**, *39* (3), 899–900.

(16) Sinha, S.; Pia Rossi, M.; Mattia, D.; Gogotsi, Y.; Bau, H. H. Induction and measurement of minute flow rates through nanopipes. *Phys. Fluids* **2007**, *19* (1), 013603.

(17) Guan, W.; Fan, R.; Reed, M. A. Field-effect reconfigurable nanofluidic ionic diodes. *Nat. Commun.* **2011**, *2* (1), 506.

(18) Daiguji, H.; Yang, P.; Majumdar, A. Ion transport in nanofluidic channels. *Nano Lett.* **2004**, *4* (1), 137–142.

(19) Schoch, R. B.; Renaud, P. Ion transport through nanoslits dominated by the effective surface charge. *Appl. Phys. Lett.* **2005**, *86* (25), 253111.

(20) Raidongia, K.; Huang, J. Nanofluidic ion transport through reconstructed layered materials. *J. Am. Chem. Soc.* **2012**, *134* (40), 16528–16531.

(21) He, Y.; Gillespie, D.; Boda, D.; Vlasiouk, I.; Eisenberg, R. S.; Siwy, Z. S. Tuning transport properties of nanofluidic devices with local charge inversion. *J. Am. Chem. Soc.* **2009**, *131* (14), 5194–5202.

(22) Fan, R.; Huh, S.; Yan, R.; Arnold, J.; Yang, P. Gated proton transport in aligned mesoporous silica films. *Nat. Mater.* **2008**, *7* (4), 303.

(23) Goldberger, J.; Fan, R.; Yang, P. Inorganic nanotubes: a novel platform for nanofluidics. *Acc. Chem. Res.* **2006**, *39* (4), 239–248.

(24) Pérez Mitta, G.; Marmisollé, W. A.; Albesa, A. G.; Toimil Molares, M. E.; Trautmann, C.; Azzaroni, O. Phosphate Responsive Biomimetic Nanofluidic Diodes Regulated by Polyamine-Phosphate Interactions: Insights into Their Functional Behavior from Theory and Experiment. *Small* **2018**, *14* (18), 1702131.

(25) Zhang, H.; Hou, X.; Hou, J.; Zeng, L.; Tian, Y.; Li, L.; Jiang, L. Synthetic Asymmetric Shaped Nanodevices with Symmetric pH Gating Characteristics. *Adv. Funct. Mater.* **2015**, *25* (7), 1102–1110.

(26) Stein, D.; Kruithof, M.; Dekker, C. Surface-charge-governed ion transport in nanofluidic channels. *Phys. Rev. Lett.* **2004**, *93* (3), 035901.

- (27) Cao, H.; Yu, Z.; Wang, J.; Tegenfeldt, J. O.; Austin, R. H.; Chen, E.; Wu, W.; Chou, S. Y. Fabrication of 10 nm enclosed nanofluidic channels. *Appl. Phys. Lett.* **2002**, *81* (1), 174–176.
- (28) Shao, J.-J.; Raidongia, K.; Koltanow, A. R.; Huang, J. Self-assembled two-dimensional nanofluidic proton channels with high thermal stability. *Nat. Commun.* **2015**, *6*, 7602.
- (29) Qin, S.; Liu, D.; Wang, G.; Portehault, D.; Garvey, C. J.; Gogotsi, Y.; Lei, W.; Chen, Y. High and stable ionic conductivity in 2D nanofluidic ion channels between boron nitride layers. *J. Am. Chem. Soc.* **2017**, *139* (18), 6314–6320.
- (30) Cheng, C.; Jiang, G.; Garvey, C. J.; Wang, Y.; Simon, G. P.; Liu, J. Z.; Li, D. Ion transport in complex layered graphene-based membranes with tuneable interlayer spacing. *Sci. Adv.* **2016**, *2* (2), No. e1501272.
- (31) Cheng, H.; Zhou, Y.; Feng, Y.; Geng, W.; Liu, Q.; Guo, W.; Jiang, L. Electrokinetic Energy Conversion in Self Assembled 2D Nanofluidic Channels with Janus Nanobuilding Blocks. *Adv. Mater.* **2017**, *29* (23), 1700177.
- (32) Ji, J.; Kang, Q.; Zhou, Y.; Feng, Y.; Chen, X.; Yuan, J.; Guo, W.; Wei, Y.; Jiang, L. Osmotic power generation with positively and negatively charged 2D nanofluidic membrane pairs. *Adv. Funct. Mater.* **2017**, *27* (2), 1603623.
- (33) Yeh, C.-N.; Raidongia, K.; Shao, J.; Yang, Q.-H.; Huang, J. On the origin of the stability of graphene oxide membranes in water. *Nat. Chem.* **2015**, *7* (2), 166.
- (34) Sun, P.; Zhu, M.; Wang, K.; Zhong, M.; Wei, J.; Wu, D.; Xu, Z.; Zhu, H. Selective ion penetration of graphene oxide membranes. *ACS Nano* **2013**, *7* (1), 428–437.
- (35) Fan, X.; Peng, W.; Li, Y.; Li, X.; Wang, S.; Zhang, G.; Zhang, F. Deoxygenation of exfoliated graphite oxide under alkaline conditions: a green route to graphene preparation. *Adv. Mater.* **2008**, *20* (23), 4490–4493.
- (36) Kim, F.; Luo, J.; Cruz Silva, R.; Cote, L. J.; Sohn, K.; Huang, J. Self propagating domino like reactions in oxidized graphite. *Adv. Funct. Mater.* **2010**, *20* (17), 2867–2873.
- (37) Zhu, H.; Luo, W.; Ciesielski, P. N.; Fang, Z.; Zhu, J.; Henriksson, G.; Himmel, M. E.; Hu, L. Wood-derived materials for green electronics, biological devices, and energy applications. *Chem. Rev.* **2016**, *116* (16), 9305–9374.
- (38) Saito, T.; Kimura, S.; Nishiyama, Y.; Isogai, A. Cellulose nanofibers prepared by TEMPO-mediated oxidation of native cellulose. *Biomacromolecules* **2007**, *8* (8), 2485–2491.
- (39) Li, T.; Li, S. X.; Kong, W.; Chen, C.; Hitz, E.; Jia, C.; Dai, J.; Zhang, X.; Briber, R.; Siwy, Z. A nanofluidic ion regulation membrane with aligned cellulose nanofibers. *Sci. Adv.* **2019**, *5* (2), No. eaau4238.
- (40) Olivier, C.; Moreau, C. I.; Bertoncini, P.; Bizot, H.; Chauvet, O.; Cathala, B. Cellulose nanocrystal-assisted dispersion of luminescent single-walled carbon nanotubes for layer-by-layer assembled hybrid thin films. *Langmuir* **2012**, *28* (34), 12463–12471.
- (41) Li, Y.; Zhu, H.; Shen, F.; Wan, J.; Lacey, S.; Fang, Z.; Dai, H.; Hu, L. Nanocellulose as green dispersant for two-dimensional energy materials. *Nano Energy* **2015**, *13*, 346–354.
- (42) Zhou, Y.; Chen, C.; Zhu, S.; Sui, C.; Wang, C.; Kuang, Y.; Ray, U.; Liu, D.; Brozena, A.; Leiste, U. H.; Quispe, N.; Guo, H.; Vellore, A.; Bruck, H. A.; Martini, A.; Foster, B.; Lou, J.; Li, T.; Hu, L. A printed, recyclable, ultra-strong, and ultra-tough graphite structural material. *Mater. Today* **2019**, DOI: 10.1016/j.mattod.2019.03.016.
- (43) Ciesielski, A.; Samori, P. Graphene via sonication assisted liquid-phase exfoliation. *Chem. Soc. Rev.* **2014**, *43* (1), 381–398.
- (44) Wei, C.; Bard, A. J.; Feldberg, S. W. Current rectification at quartz nanopipet electrodes. *Anal. Chem.* **1997**, *69* (22), 4627–4633.
- (45) Chen, G. H.; Wu, D. J.; Weng, W. G.; Yan, W. L. Preparation of polymer/graphite conducting nanocomposite by intercalation polymerization. *J. Appl. Polym. Sci.* **2001**, *82* (10), 2506–2513.
- (46) Chen, G.; Wu, C.; Weng, W.; Wu, D.; Yan, W. Preparation of polystyrene/graphite nanosheet composite. *Polymer* **2003**, *44* (6), 1781–1784.
- (47) Srivastava, N.; Mehra, R. Study of structural, electrical, and dielectric properties of polystyrene/foiled graphite nanocomposite developed via in situ polymerization. *J. Appl. Polym. Sci.* **2008**, *109* (6), 3991–3999.
- (48) Du, X.; Xiao, M.; Meng, Y.; Hay, A. Synthesis and properties of poly (4, 4'-oxybis (benzene) disulfide)/graphite nanocomposites via in situ ring-opening polymerization of macrocyclic oligomers. *Polymer* **2004**, *45* (19), 6713–6718.
- (49) Wen Ping, W.; Cai Yuan, P. Preparation and characterization of poly (methyl methacrylate) intercalated graphite oxide/poly (methyl methacrylate) nanocomposite. *Polym. Eng. Sci.* **2004**, *44* (12), 2335–2339.
- (50) Chen, L.; Shi, G.; Shen, J.; Peng, B.; Zhang, B.; Wang, Y.; Bian, F.; Wang, J.; Li, D.; Qian, Z. Ion sieving in graphene oxide membranes via cationic control of interlayer spacing. *Nature* **2017**, *550* (7676), 380.
- (51) Ober, T. J.; Foresti, D.; Lewis, J. A. Active mixing of complex fluids at the microscale. *Proc. Natl. Acad. Sci. U. S. A.* **2015**, *112* (40), 12293–12298.
- (52) Siqueira, G.; Kokkinis, D.; Libanori, R.; Hausmann, M. K.; Gladman, A. S.; Neels, A.; Tingaut, P.; Zimmermann, T.; Lewis, J. A.; Studart, A. R. Cellulose nanocrystal inks for 3D printing of textured cellular architectures. *Adv. Funct. Mater.* **2017**, *27* (12), 1604619.
- (53) Agmon, N. The grotthuss mechanism. *Chem. Phys. Lett.* **1995**, *244* (5–6), 456–462.
- (54) Ordinario, D. D.; Phan, L.; Walkup IV, W. G.; Jocson, J.-M.; Karshalev, E.; Hüsken, N.; Gorodetsky, A. A. Bulk protonic conductivity in a cephalopod structural protein. *Nat. Chem.* **2014**, *6* (7), 596.

SUPPLEMENTARY INFORMATION

Decoupling ionic and electronic pathways in low-dimensional hybrid conductors

Yubing Zhou,^{1,†} Chaoji Chen,^{1,†} Xin Zhang,^{1,†} Dapeng Liu,¹ Lisha Xu,¹ Jiaqi Dai,¹ Sz-Chian Liou,² Yilin Wang,¹ Claire Li,¹ Hua Xie,¹ Qingyun Wu,¹ Bob Foster,³ Teng Li,⁴ Robert M. Briber,¹ Liangbing Hu^{1*}

1. Department of Materials Science and Engineering, University of Maryland, College Park, Maryland, 20742
2. Advanced Imaging and Microscopy (AIM) Lab of Nano Center, University of Maryland, College Park, 20742
3. Trinity Industries, Inc., Dallas, Texas, 75207.
4. Department of Mechanical Engineering, University of Maryland, College Park, MD 20742.

* Email: binghu@umd.edu

†These authors contributed equally to this work.

Methods

Preparation process of graphite-NFC slurry

NFC fibers with negatively charged carboxyl groups were produced by (2,2,6,6-tetramethylpiperidin-1-yl)oxidanyl (TEMPO) oxidation. A total of 5 g of Kraft bleached hardwood (Eucalyptus) pulp was suspended in 250 mL deionized water containing 0.5 mmol TEMPO (Sigma-Aldrich, 99%) and 5 mmol NaBr (Sigma-Aldrich, $\geq 99.99\%$). The TEMPO mediated oxidation is initiated with the addition of 25 mmol NaClO. The pH is maintained at 10.0 with 1 mol/L NaOH solution. The whole oxidation process is maintained under stirring (IKA RW20 digital mixer) for 2-3 h. The resulting pulp was then washed by filtration and stored at 4 °C for further analysis and treatment. The diameter of the resulting fibers was further reduced by mechanical treatment in a microfluidizer (M-110EH Microfluidizer Processor) at pressures of 20,000 psi.

To make graphite-NFC slurry with a mass ratio of 1:1, commercial graphite powder (Asbury Carbons 3061) and obtained NFC solution were mixed together with a solid mass ratio of 1:1 for graphite to NFC. The dispersion process was performed using a Vibra-Cell ultrasonic liquid processor for 5 min, and then bath sonicated for 15 min (FS110D, Fisher Scientific). After sonication, the graphite flakes were well dispersed in the NFC solution. More details about graphite-NFC slurry making process can be found in our previous article ¹.

3D printing

3D printing fabrication was conducted using a benchtop robot (Fisnar F4200n), which was controlled by programmed procedures. The graphite-NFC slurry was placed into a syringe tube with a 305 μm tip diameter for the printing process. An air-driven fluid dispenser (DSP501N, Fisnar) provided appropriate pressure (30-50 psi) to extrude the slurry onto a glass slide. After

printing, the samples of various geometries were transferred into a constant temperature humidity chamber (LHS-150HC-II, set to 40 °C, 40% RH) for 3 h to remove water.

Characterization

The graphite-NFC composite was embedded in epoxy and microtomed at room temperature under either dry or wet conditions with a diamond knife. The section was ~100 nm thick. TEM observation was conducted with a JEOL JEM-2100 TEM at 200kV acceleration voltage and equipped with a Gatan Tridiem 863 GIF (Gatan Imaging Filter) system. All the high resolution TEM images were recorded under the Scherzer defocus condition. SEM images were taken with a Hitachi SU-70 Schottky field emission gun scanning electron microscope (2-5 kV, depending on the sample state). All samples were coated by gold sputtering for 90 s prior to observation. The Zeta potential was determined using a Zetasizer Nano ZS90. TGA data were collected with a TA instrument (SDT650) from room temperature to 800 °C at a heating rate of 3 °C/min in air atmosphere.

Conductivity Measurement of the ionic conductors

The dry and fully swollen graphite-NFC films were cut into a rectangular shape. Then the films were sealed in hard epoxy to remain the thickness unchanged. The two ends of the film were exposed to ensure good contact with the electrodes. The as-made nanofluidic devices were soaked in different concentrations of NaCl solution for conductivity measurements. At each concentration, the devices were soaked more than 24 h to reach equilibrium. The conductivity measurements were conducted with a BioLogic VMP3 potentiostat. Two Ag/AgCl electrodes were attached to the two ends of the nanofluidic device as the electrodes. I-V curves of ionic conductors were recorded at various electrolyte concentrations from 10^{-6} M to 1 M.

References

1. Zhou, Y.; Chen, C.; Zhu, S.; Sui, C.; Wang, C.; Kuang, Y.; Ray, U.; Liu, D.; Brozena, A.; Leiste, U. H.; Quispe, N.; Guo, H.; Vellore, A.; Bruck, H. A.; Martini, A.; Foster, B.; Lou, J.; Li, T.; Hu, L. A printed, recyclable, ultra-strong, and ultra-tough graphite structural material. *Mater. Today* **2019** DOI:10.1016/j.mattod.2019.03.016.

Supplementary figures

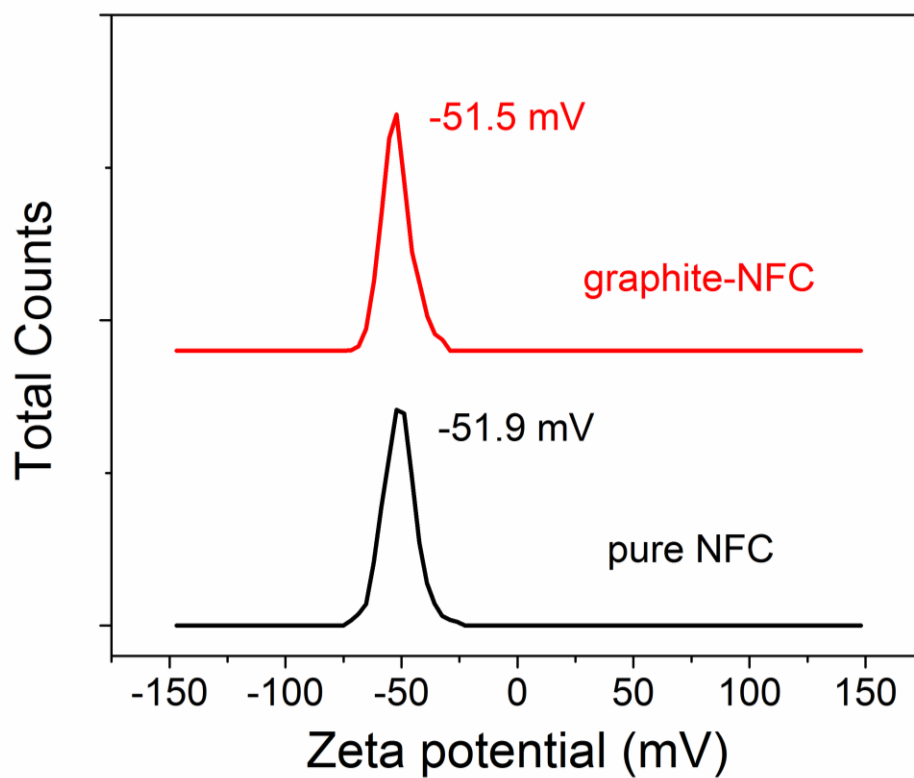


Figure S1. Zeta potential of pure NFC and graphite-NFC slurry.

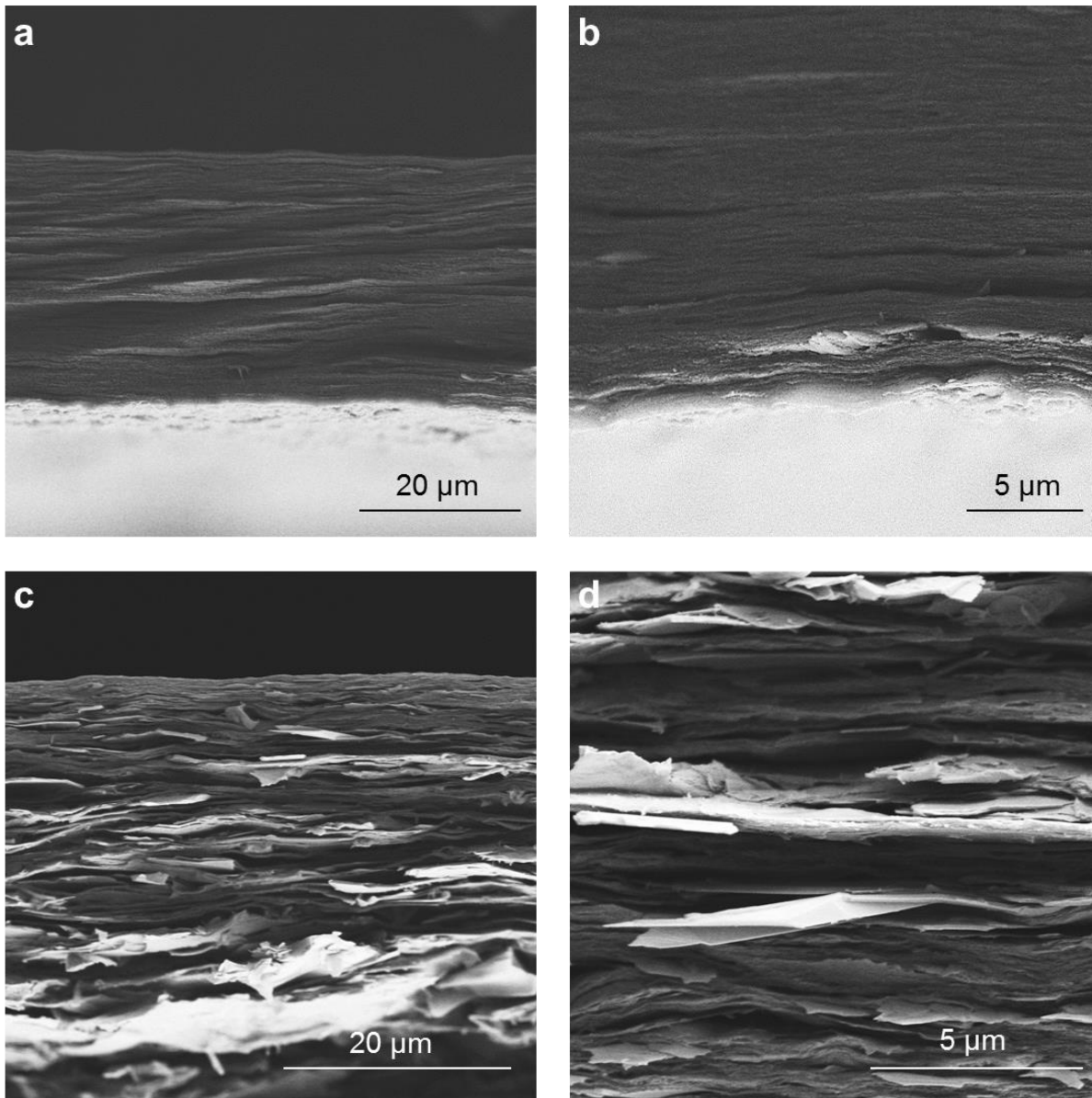


Figure S2. (a,b) Cross-sectional SEM images of pure NFC paper, and (c,d) the graphite-NFC membrane.

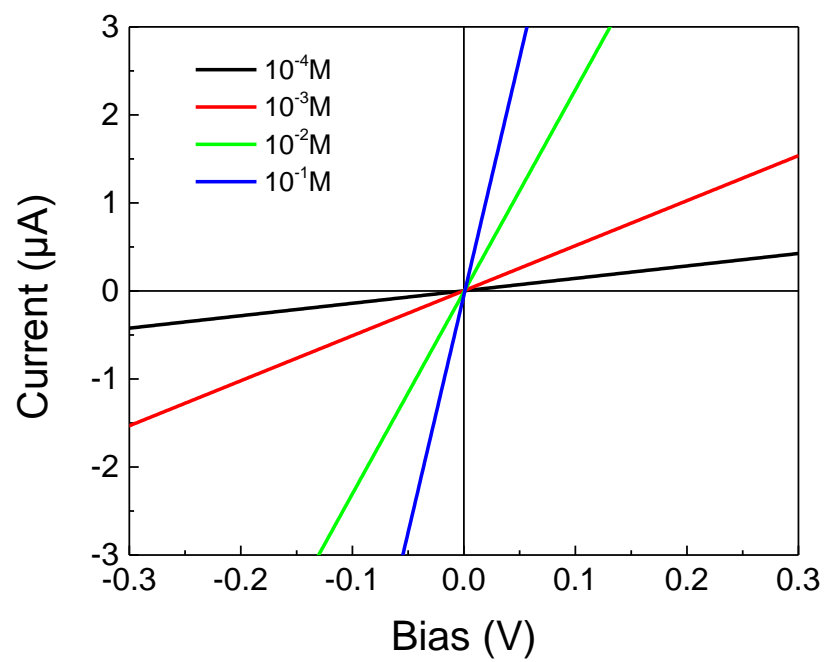


Figure S3. Representative I-V curves of the confined graphite-NFC membrane at different NaCl concentrations.

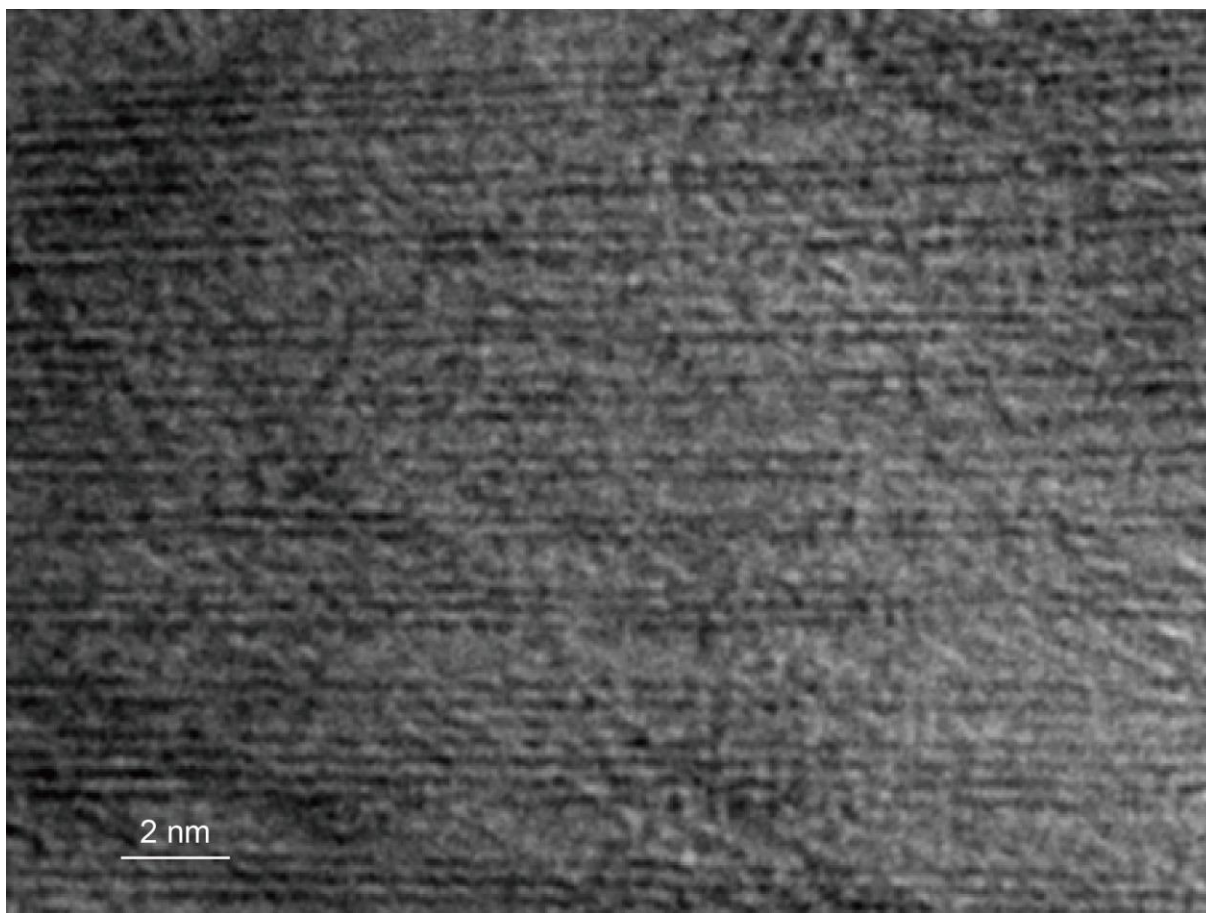


Figure S4. High resolution TEM image of the exfoliated graphite flake shown in Figure 4c.

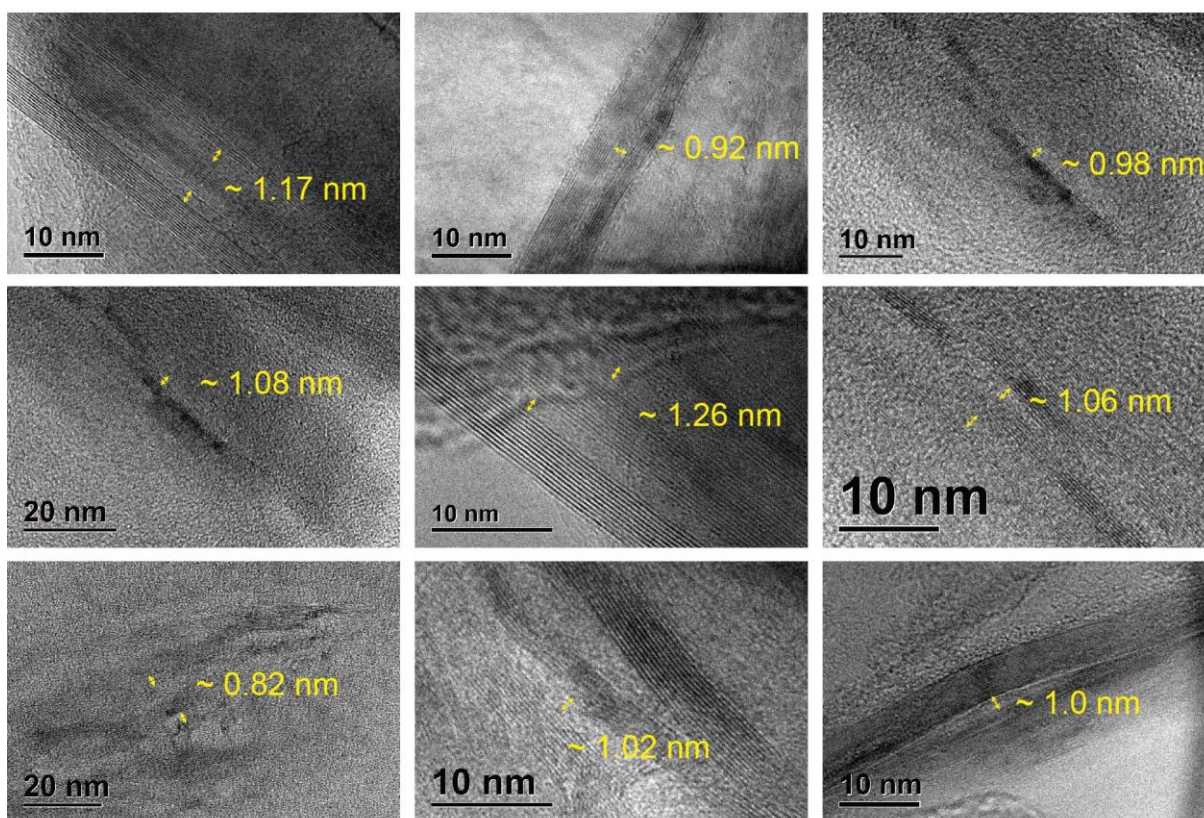
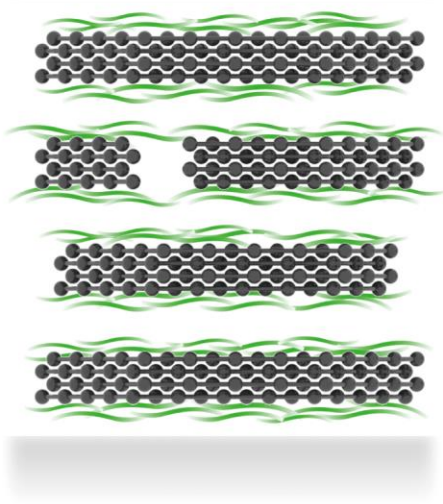


Figure S5. High resolution TEM images of ultrathin sections of graphite-NFC membranes in confined hydrated state embedded in epoxy. The actual spacing between the flakes can be observed clearly.

a confined hydrated membrane



b confined hydrated membrane without sonication

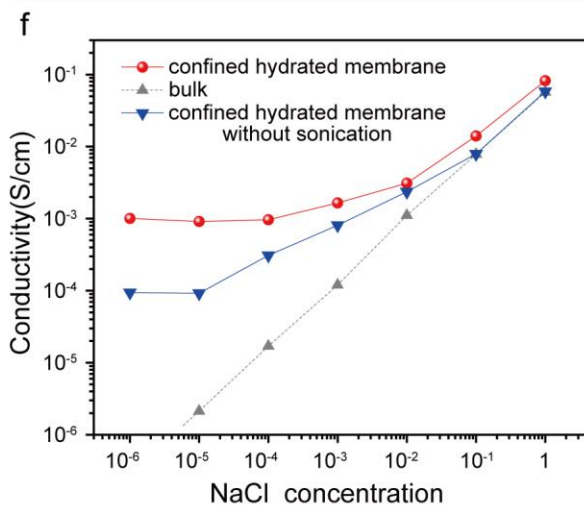
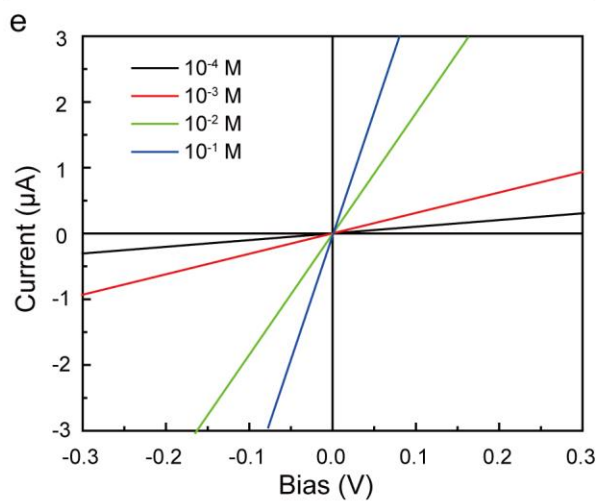
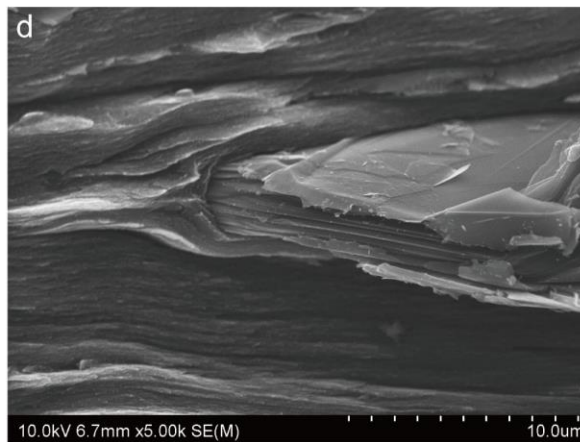
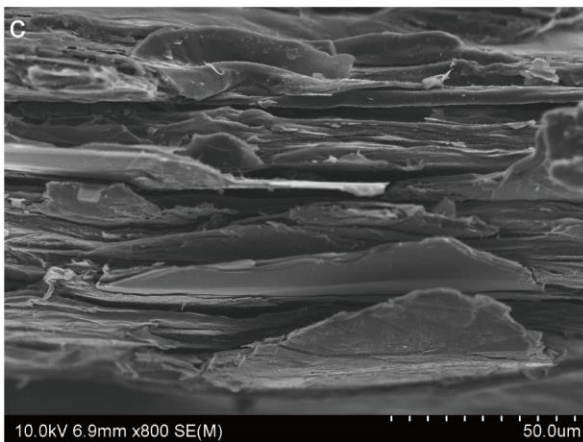
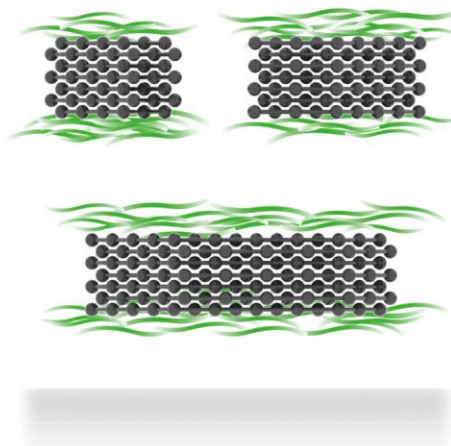


Figure S6. (a, b) Schematics of the nanofluidic channels of the graphite-NFC membrane (a) with sonication and (b) without sonication. (c, d) Cross-sectional SEM image of the graphite-NFC membrane made without sonication. (e) Representative I-V curves of the confined hydrated graphite-NFC membrane without sonication at different NaCl concentrations. (f) The ionic conductivity as a function of electrolyte concentration at different NaCl concentrations. The blue and red lines are the ionic conductivities of the confined hydrated graphite-NFC membranes with and without sonication, respectively.

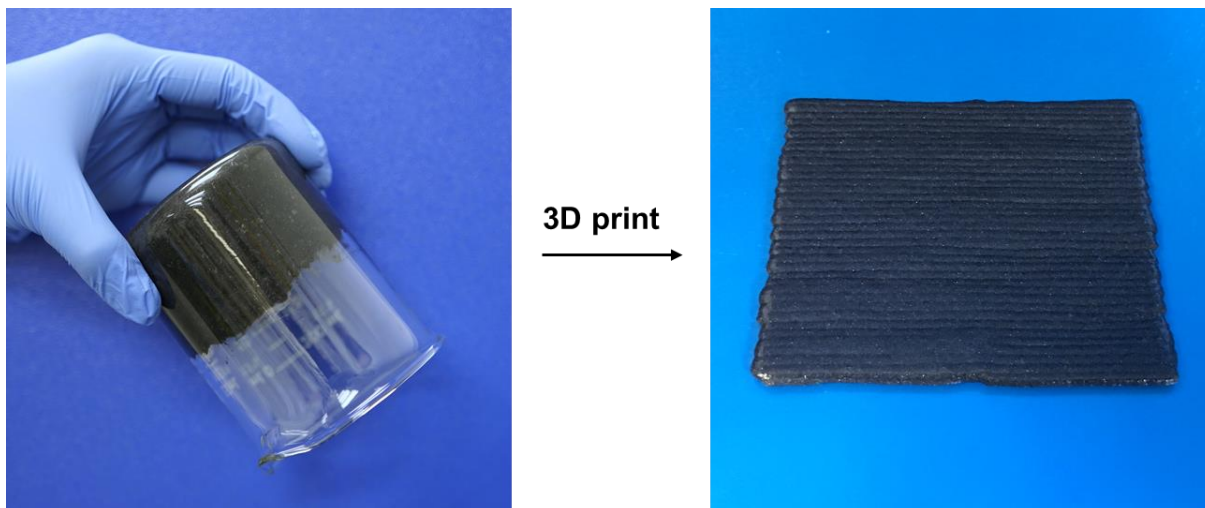


Figure S7. The graphite-NFC slurry with a solid content of 20 wt.% shows ideal gel-like behavior and superior filament shape retention after extrusion by 3D printing.

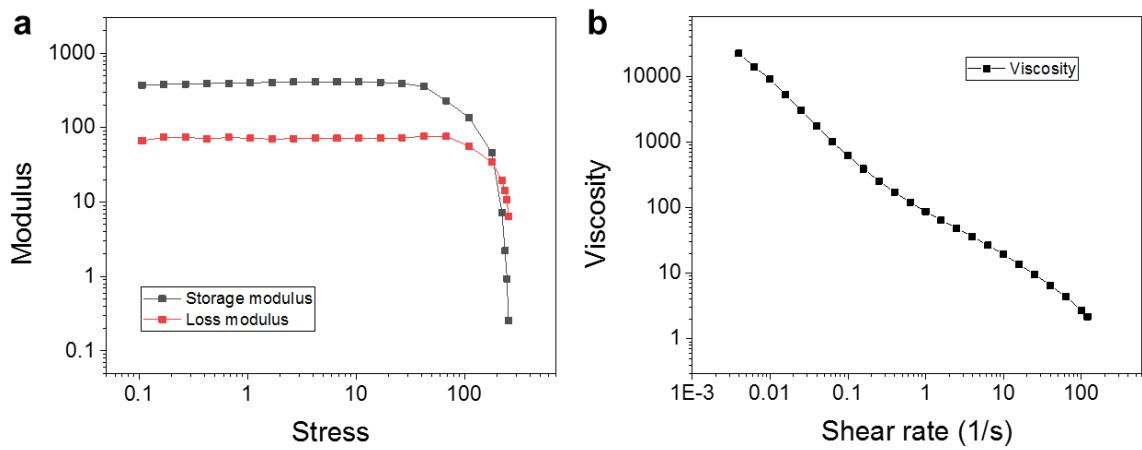


Figure S8. (a) Storage modulus and loss modulus as a function of shear stress for graphite-NFC slurry. Typical viscoelastic property is suitable for extrusion-based 3D printing. (b) Apparent viscosity as a function of shear rate for graphite-NFC slurry.

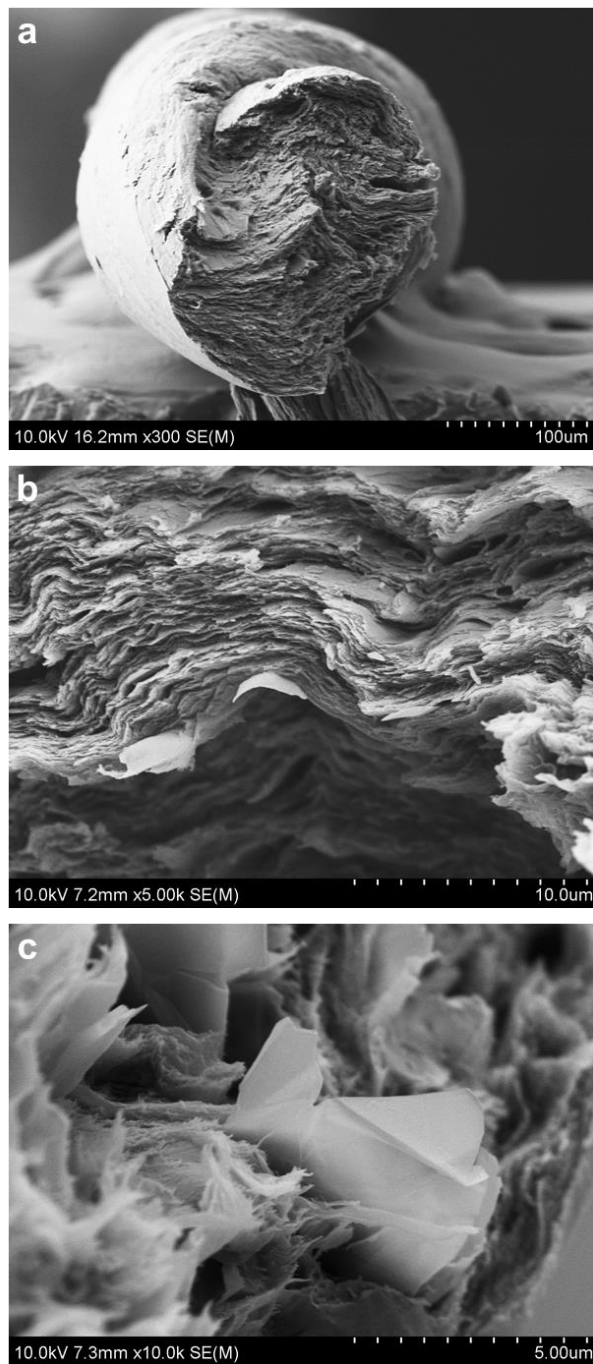


Figure S9. (a) Low-magnification and (b, c) high-magnification cross-section SEM images of the graphite-NFC fiber.

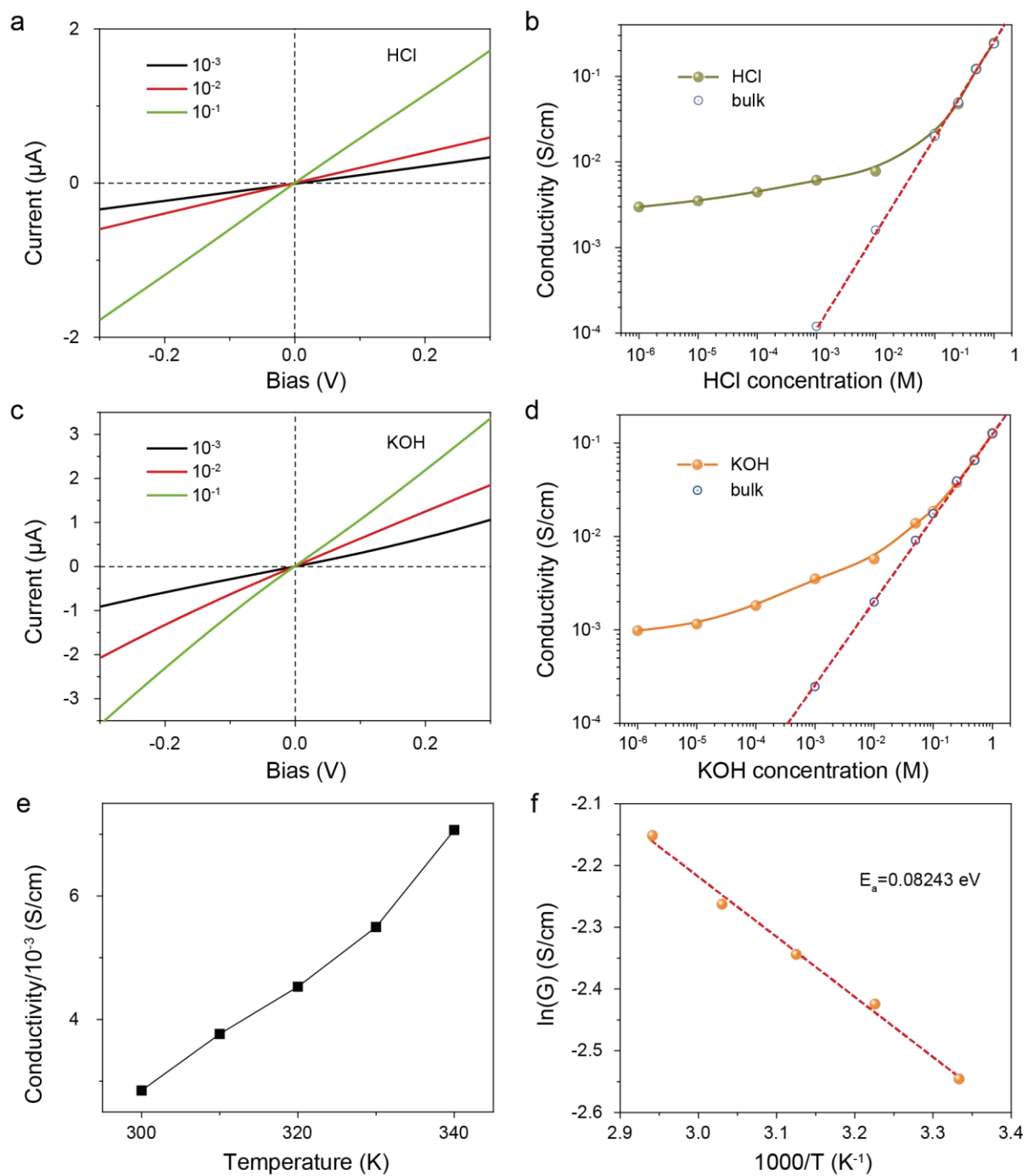


Figure S10. Ionic conductivity tests of graphite-NFC membrane-based nanofluidic devices were carried out at various HCl or KOH concentrations (up to 1 M) respectively. (a) I–V curves obtained at HCl concentrations of 0.001, 0.01, and 0.1 M. (b) Ionic conductivity as a function of the HCl concentration. (c) I–V curves obtained at KOH concentrations of 0.001, 0.01, and 0.1 M. (d) Ionic

conductivity as a function of the KOH concentration. (e) Ionic conductivity of the graphite-CNF film at different temperatures. (f) Arrhenius plot of the conductance ($\ln(G)$) vs. inverse temperature ($1000/T$) for the graphite-NFC film.

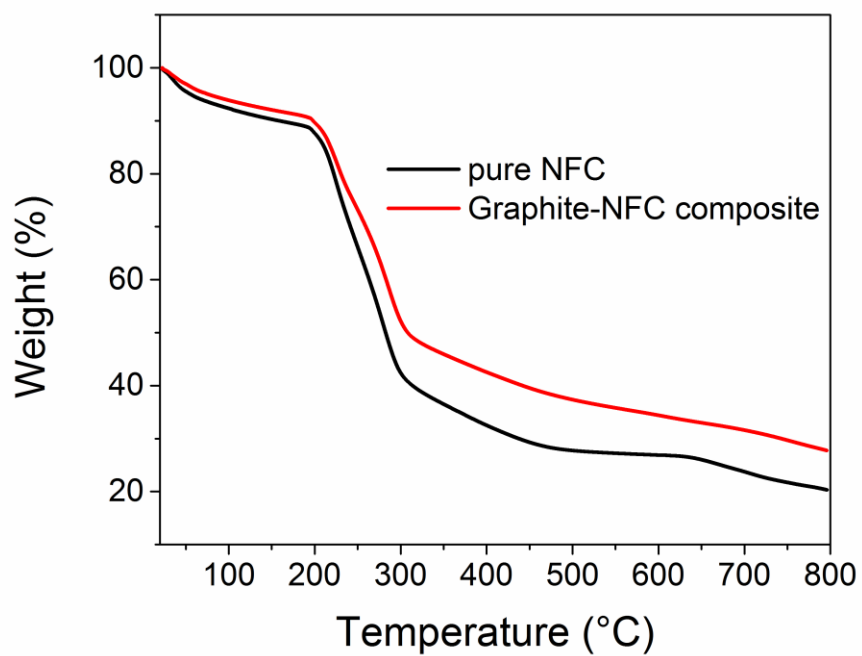


Figure S11. Thermogravimetric curves showing the thermal degradation of graphite-NFC composite and pure NFC.